Available online at www.sciencedirect.com
ScienceDirect
Journal of Power Sources 179 (2008) 177–185
JOURNAL OF POWER SOURCES
www.elsevier.com/locate/jpowsour

High performance electrolyte-coated anodes for low-temperature solid oxide fuel cells: Model and Experiments

Dong Ding, Wei Zhu, Jianfeng Gao, Changrong Xia *

Laboratory for Renewable Clean Energy, Department of Materials Science and Engineering, University of Science and Technology of China, 96 Jinzhai Road, Hefei, 230026 Anhui, China

Received 22 November 2007; received in revised form 16 December 2007; accepted 18 December 2007
Available online 26 December 2007

Abstract

A geometric micro-model and experiment development are presented for electrolyte-coated anodes with high performance in solid oxide fuel cells. The anodes are based on electron conducting frameworks, where fine, oxygen-ion conducting inclusions are introduced via an ion impregnation process. The model shows that the length of triple-phase-boundary (TPB) increases with the loading of the coated electrolyte, and is dependent only on the loading before a maximum loading for monolayer coverage is obtained. The maximum loading increases with the porosity of the framework. As a result, the prolonged TPB length can be achieved by increasing the porosity and the loading. In the experimental study, Ni was used as the electron conductor, and samaria-doped ceria (SDC) was employed as the electrolyte to form anode-supported single cells. The cell performance was evaluated using humidified hydrogen as the fuel. The peak power density increased with SDC loading to a maximum value and decreased when the loading was further increased. The highest peak power density of the cells whose anodes were prepared with 10, 20 and 30 wt.% pore former was 571, 631 and 723 mW cm^{-2}, corresponding to 508, 564 and 648 mg cm^{-3} of SDC loading, respectively. The experimental results are in good agreement with the model prediction. Therefore, this work demonstrates theoretically and experimentally that optimization of the porosity and electrolyte loading is critical for further improving the performance of electrolyte-coated anodes.
© 2007 Elsevier B.V. All rights reserved.

Keywords: Electrolyte-coated anode; Geometric micro-model; Ion impregnation process; Doped ceria; Solid oxide fuel cells

1. Introduction

Recently, there have been lots of interests in improving the performance of electrodes for solid state fuel cells (SOFCs) to lower their operating temperatures [1]. In the case of the anodes, most researches were focused on the micro-structure optimization via catalyst surface modification [2–5]. One of the practices is to coat fine particles of electrolyte such as yttria-stabilized zirconia (YSZ) and doped ceria on an electron conducting matrix phase of Ni-based porous materials. One advantage of the electrolyte-coated anodes is that they are capable of effectively suppressing carbon deposition when hydrocarbon is directly used as the fuel [4,6–8]. The other advantage is that the anodic performance is significantly improved by coating the fine electrolyte particles, which are usually introduced using an ion impregnation process [3]. Jiang et al. have shown that the performance of Ni-based anodes could be substantially improved by coating nano-sized electrolyte particles of YSZ and gadolinia-doped ceria (GDC). At 700 °C, the interfacial polarization resistance of an uncoated anode was 10 Ω cm^2. It was reduced to 3.1 Ω cm^2 when 4.0 mg cm^{-2} of YSZ was impregnated [9]. The resistance was further reduced to 0.71 Ω cm^2 when the electrode was coated with 1.7 mg cm^{-2} of GDC [10]. Zhu et al. [7] have also demonstrated that a significant reduction of the interfacial polarization resistance was achieved when 20 mg cm^{-2} of samaria-doped ceria (SDC) was coated into NiO-based anode substrate. In addition, distinct improvement in performance was observed for single cells with the electrolyte-coated anodes, compared with that of the cells without impregnation treatment. The improved performances are usually attributed to an effective extension of the triple-phase-boundary (TPB) area, in addition to significant electro-catalytic

Abbreviations: TPB, triple-phase-boundary; SDC, samaria-doped ceria; SOFC, solid oxide fuel cell; YSZ, yttria-stabilized zirconia; GDC, gadolinia-doped ceria.

* Corresponding author. Tel.: +86 551 3607475; fax: +86 551 3606689.
E-mail addresses: dingdong@mail.ustc.edu.cn (D. Ding), zhuweim@mail.ustc.edu.cn (W. Zhu), jfgao@ustc.edu.cn (J. Gao), xiacr@ustc.edu.cn (C. Xia).

0378-7753/$ – see front matter © 2007 Elsevier B.V. All rights reserved.
doi:10.1016/j.jpowsour.2007.12.059

Nomenclature

A_c	the surface area of the hypothetical sphere is occupied by an i-particle (m^2)
A_d	the disappeared surface area of an e-particle due to the contact with another e-particle (m^2)
A_E	the exposed surface area of e-particles per unit volume ($m^2\,m^{-3}$)
A_e^0	the surface area of a free-standing e-particle (m^2)
E_N	Nernst potential (V)
L_{TPB}	the length of triple-phase-boundary
m	loading ($mg\,cm^{-3}$)
n_e	the number of e-particles per unit volume
N_i	the number of i-particles which could be covered on the exposed surface of e-particles per unit volume
N_i^0	the number of i-particles which could be covered on the surface of one free-standing e-particle with a monolayer
P_c	the critical probability of infinitely long sequences of adjacent sites for i-particles
r	radius of a particle (μm)
R_o	intercept with the real axis at high frequency in impedance spectra ($\Omega\,cm^2$)
R_p	interfacial polarization resistance of a single cell ($\Omega\,cm^2$)
R_t	intercept with the real axis at low frequency in impedance spectra ($\Omega\,cm^2$)
V_{oc}	open circuit voltage (V)
Z	co-ordination number

Greek letters

ε	open porosity
λ	fractional coverage
θ_1	one half of the contact angle between two e-particles (°)
θ_2	one half of the contact angle between an e-particle and an i-particle (°)
ρ	density ($g\,cm^{-3}$)
φ	critical volume fraction of i-particles in all particles for a two dimensional system
ϕ	a factor

Subscripts

cr	critical
h	hypothetical
i	ion conducting particle
e	electron conducting particle

effect of coating nano-sized electrolyte particles on the electrochemical activity of the anode [3]. It is well known that TPB in a composite electrode is the active site for electrode reaction, where electron conducting phase (Ni), ion conducting phase (YSZ) and gas phase (H_2 and product water vapor) meet. The TPB length plays an important role in determining the electrode performance. As demonstrated by Mizusaki et al. [11] and Bieberle and Gauckler [12], the electrode performance of a Ni-based anode was directly related to the TPB length, which has been shown to be determined by micro-structural parameters such as grain size, pore diameter and porosity [13] as well as the size ratio of electronic and ionic phase particles [14]. From this point of view, the surface modification is to achieve the TPB length per unit volume as large as possible by optimizing one or more parameters. However, no model is available to predict the modification effect with regards to TPB up to now.

Anyway, several models have been proposed to investigate the correlation between the micro-structural parameters and the performance of conventional composite electrodes in order to provide fundamental information for micro-structure design [15–17]. In a random packing micro-model, TPBs are formed by the contacts of percolated electronic and ionic phase particles and thus depend not only on micro-structure characteristics of the particles such as the number of each particle per unit volume and the co-ordination number but also on the probability of each phase particle belonging to the percolated cluster [18,19]. Therefore, the determination of TPB length is quite complex. In Deng's geometrical model [13], only the relative value of TPB length was calculated. For an electrolyte-coated anode, this issue seems to be somewhat different and can probably be simplified. The reason lies on the following facts: (1) the fine coated particles do not belong to the random packing system in a three dimensional space. Instead, the particles form a continuous phase for oxygen-ion conduction on the surface of the particles belonging to the porous matrix based on Ni; (2) the difference of the size of the two phase particles is in the level of magnitude, which is much larger than the difference for a conventional composite anode. Further, there exists an important fact that the exposed surface of matrix phase particles per unit volume, i.e. the available surface for coating, is determined by the average number of matrix phase particles and the average co-ordination number between matrix phase particles, which both are dependent on the porosity. Therefore, it is necessary to develop a new model and correlative experiment to investigate the micro-structure effect on the electrode performance and optimize the fabrication parameters for the electrolyte-coated anode.

In this work, a geometrical micro-model was developed for electrolyte-coated anodes. The TPB length per unit volume was predicted as a function of the porosity and the amount of coated electrolyte. In addition, the performance of single cells based on the electrolyte-coated anodes was experimentally investigated concerning the porosity and electrolyte loadings. The anode was based on an electron conducting Ni framework that was coated with ion conducting phase of SDC. The experimental results were in good agreement with the model predictions.

2. Geometrical micro-model for an electrolyte-coated anode

As shown in Fig. 1a, an electrolyte-coated anode is composed of an electron conducting framework and coating layer of oxygen-ion conducting particles (hereafter they will be referred

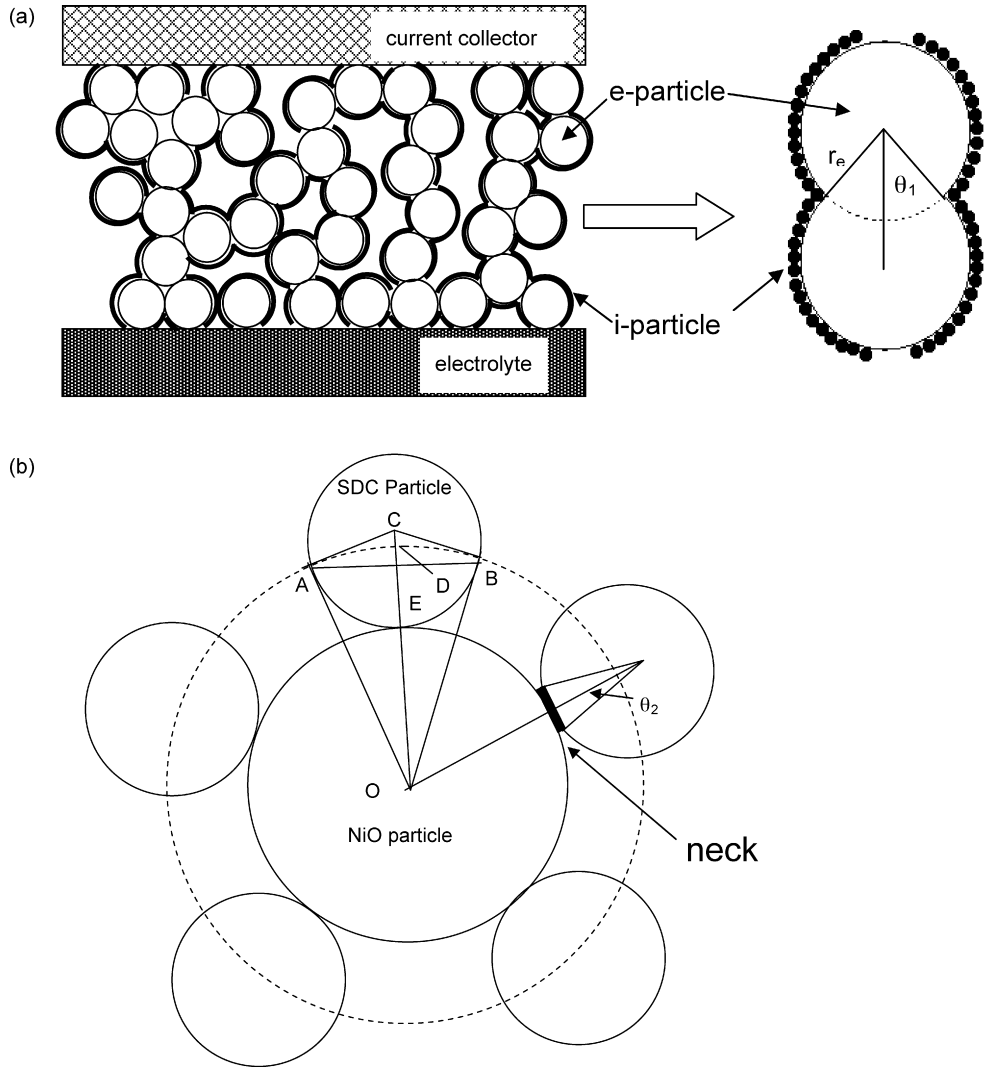

Fig. 1. Schematic diagrams for (a) the micro-structure of an electrolyte-coated anode and (b) an electronic conductor particle (e-particle) in direct contact with ionic conductor particles (i-particle).

to as i-particles). The framework is fabricated with a conventional ceramic processing method such as dry-pressing and tape-casting. Those i-particles are subsequently deposited on the surface of the particles belonging to the framework using an ion-impregnation technique. Since the framework is formed before the impregnation process, the electron conducting materials can be reasonably assumed to constitute a percolated system for all particles (hereafter they will be referred to as e-particles). Those e-particles are further assumed to be spheres with equal radius of r_e and to be randomly packed to form the framework. The formation has to be processed at high temperature to strength the bonding between the e-particles. As a result, the surface area reduces due to sintering. For an e-particle, the disappeared surface area, A_d, due to the contact with another e-particle, can be obtained with the following equation:

$$A_d = 2\pi r_e^2(1 - \cos\theta_1) \tag{1}$$

where θ_1 is one half of the contact angle of two e-particles as shown in Fig. 1a, and r_e is the radius of e-particle.

The number of e-particles per unit volume in the electron conducting framework, n_e, is given by the following equation:

$$n_e = \frac{1-\varepsilon}{(4/3)\pi r_e^3} \tag{2}$$

where ε is the porosity of the anode framework.

The exposed surface area of e-particles per unit volume, i.e. the surface area that is available for the coverage of i-particles, A_E, is given by the following equation:

$$A_E = A_e^0 n_e - A_d n_e Z \tag{3}$$

where $A_e^0 = 4\pi r_e^2$, is the surface area of a free-standing e-particle and Z is the average co-ordination number, which is a function of the porosity. According to Ref. [20], Z can be empirically expressed as

$$Z = 20.7(1-\varepsilon) - 4.35 \quad \text{when } 0.3 \le \varepsilon \le 0.53 \tag{4}$$

and

$$Z = 36(1-\varepsilon)/\pi \quad \text{when } 0.53 \le \varepsilon \tag{5}$$

combining Eqs. (1)–(5), at $0.3 \leq \varepsilon \leq 0.53$, A_E is given as

$$A_E = -\frac{3}{2r_e}(20.7(1-\cos\theta_1)\varepsilon^2 - (35.05 - 37.05\cos\theta_1)\varepsilon - 16.35\cos\theta_1 + 14.35) \quad (6)$$

and at $0.53 \leq \varepsilon$

$$A_E = -\frac{3}{2\pi r_e}(36(1-\cos\theta_1)\varepsilon^2 - (72 - 72\cos\theta_1 - 2\pi)\varepsilon - (36\cos\theta_1 + 2\pi - 36)) \quad (7)$$

Now let us consider N_i^0, the number of i-particles which are fully covered on the surface of one free-standing e-particle with a monolayer. A hypothetical sphere with radius r_h = OD is presented (Fig. 1b). Based on the fact that r_i is about one magnitude lower than r_e, we assume that the decrease of distance between the two-circle centers due to sintering is negligible. As shown in Fig. 1b, part of the surface area of the hypothetical sphere is occupied by an i-particle. This occupied area, A_c, can be geometrically calculated by the following equation [21]:

$$A_c = 2\pi\left[-\frac{\{r_e(r_e+2r_i)\}^{3/2}}{r_e+r_i} + r_e(r_e+2r_i)\right] \quad (8)$$

where r_e = OE and r_i = CE, respectively. Therefore, N_i^0, can be obtained by approximating r_i = DE, as

$$N_i^0 = \frac{4\pi(r_e+r_i)^2 \times 0.907}{A_c} \quad (9)$$

where 0.907 is the maximum packing fraction in a two dimensional system for close packing spheres. When part of the exposed surface area per unit volume is covered by the i-particles, the number of i-particles per unit volume, N_i, is

$$N_i = \lambda N_i^0 \frac{A_E}{4\pi r_e^2} \quad (10)$$

where λ is the fractional coverage, which is obviously related to the loading, m_i. When e-particles are covered with a monolayer of i-particles, it gives

$$\lambda = \frac{A_i}{A_E \times 0.907} = \frac{3m_i}{4r_i\rho_i A_E \times 0.907} \quad (11)$$

where A_i is the surface area occupied by all coated i-particles and ρ_i the density of i-particle.

It is clear that all of the e-particles belong to a percolated cluster. In practice, the average size of i-particles is usually less than 100 nm while it is around 1 μm for e-particles. When the amount of i-particles is large enough, i.e. λ is large enough, i-particles form a continue oxygen-ion conducting phase. The critical coverage value, λ_{cr}, can be estimated as

$$\lambda_{cr} = \frac{3m_{cr}}{4r_i\rho_i A_E \times 0.907} \quad (12)$$

where m_{cr} is the critical loading. With Malliaris and Turner's model [22], critical volume fraction of the i-particles in all particles for a two dimensional system, φ_i, can be estimated with the following equation:

$$\varphi_i = \frac{1}{2}P_c\left[1 + \left(\frac{\phi}{4}\right)\left(\frac{r_e}{r_i}\right)\right]^{-1} \quad (13)$$

where P_c is the critical probability of infinitely long sequences of adjacent sites for i-particles. ϕ is a factor which depends on the mode of packing of the i-particle. If we assume that i-particles constitute a random packing system on the surface of e-particles and co-ordination number is 6, the value of P_c and ϕ is given to be 1/3 and 1.110, respectively [22]. In a two dimensional system, φ_1 can be also written as

$$\varphi_i = \frac{A_i}{A_E} = \frac{3m_{cr}}{4r_i\rho_i A_E} \quad (14)$$

Therefore, λ_{cr} and m_{cr} can be obtained by combining Eqs. (12)–(14).

When λ is not less than λ_{cr}, the length of the two-phase-boundary per unit volume can be given by the following equation:

$$L_{TPB} = 2\pi r_i(\sin\theta_2)N_i = \frac{r_i}{2r_e^2}\lambda N_i^0 A_E \sin\theta_2 \quad (15)$$

where θ_2 is one half of contact angle between an i-particle and an e-particle. For the monolayer coverage, gas is always available for two-phase-boundary. Therefore, L_{TPB} can be used to present the length of the triple-phase-boundary. Combining Eqs. (11) and (15) gives

$$L_{TPB} = \frac{3}{8\rho_i r_e^2}N_i^0(\sin\theta_2)m_i \quad (16)$$

3. Experimental

Ni was used as the electron conducting framework and $Sm_{0.2}Ce_{0.8}O_{1.9}$ (SDC) as the ionic conductor that was coated on the framework using an ion impregnation process. The preparation process of single cells, which were consisted of NiO–SDC anode substrates, SDC electrolytes, and $Sm_{0.5}Sr_{0.5}CoO_3$ (SSC)–SDC cathodes, and the impregnation method were described in detail in previous work of our laboratory [7].

All of the powders involved in this experiment, such as NiO, SDC and SSC were synthesized using a glycine–nitrate method. Taking the synthesis of SDC powers as an example, a solution containing Sm^{3+} and Ce^{4+} was prepared by dissolving $Sm(NO_3)_3$ and $Ce(NH_4)_2(NO_3)_6$ into distilled water with molar ratio of Sm^{3+}:Ce^{4+} = 1:4. After glycine was added, the solution was heated till self-combustion occurred. The resulted ash was calcined at 600 °C for 2 h and 800 °C for 4 h to form SDC powders, which were used for the electrolytes and electrodes, respectively. NiO and SSC ashes were both calcined at 850 °C for 4 h. Bi-layer pellets consisted of porous NiO–SDC substrates and dense SDC electrolytes were fabricated by a co-pressing process [23]. NiO was mechanically mixed with 10 wt.% of SDC to form oxide mixtures as the precursor for the substrates. The

Table 1
The loading (mg cm^{-3}) for FC10, FC20 and FC30 after several impregnating–heating cycles

Sample	Cycle	Loading	Sample	Cycle	Loading	Sample	Cycle	Loading
FC10-0	0	0	FC20-0	0	0	FC30-0	0	0
FC10-5	5	381 ± 5.1	FC20-4	4	384 ± 4.5	FC30-3	3	389 ± 4.3
FC10-7	7	508 ± 5.1	FC20-5	5	474 ± 4.5	FC30-4	4	519 ± 4.3
FC10-9	9	635 ± 5.1	FC20-6	6	564 ± 4.5	FC30-5	5	648 ± 4.3
			FC20-7	7	655 ± 4.5	FC30-6	6	778 ± 4.3

use of SDC was to enhance the adherence between the substrates and the electrolytes. To increase the substrate porosity, which is critical for the ion-impregnation process, 10, 20 and 30 wt.% of starch was added to the oxide mixtures. Thereinafter we called these cells with 10, 20 and 30wt.% starch pore former as FC10, FC20 and FC30, respectively. The starch was mechanically mixed with the oxide precursor and pre-pressed to form green substrates. A layer of SDC powders were subsequently distributed over the green substrate and uniaxially pressed at 300 MPa to form a green bi-layer. The bi-layer was co-fired at 1250 °C in air for 5 h to densify the SDC electrolyte. The thickness of the dense electrolyte was about 35 μm and that of the porous substrate was between 0.45 and 0.47 mm. The diameter of the fired pellets was 11.2 mm.

Impregnation solution with cation concentration of 1.0 mol L^{-1} was prepared by dissolving $Sm(NO_3)_3$ and $Ce(NO_3)_3$ into distilled water with molar ratio of Sm^{3+}:Ce^{3+} = 1:4. The solution was dropped onto the porous substrate under vacuum. After drying, it was heated at 800 °C for 2 h to form SDC oxide. The loading of SDC was determined by weighing the sample before impregnating and after heating. The impregnating–heating cycle was repeated to increase the SDC loading. The amount of impregnated SDC resulted with each cycle was different for the substrates with different porosity and slightly decreased with increased cycles. The loading for FC10, FC20 and FC30 at different cycles were listed in Table 1. The Archimedes method was used for measuring the porosity.

After impregnation, cathode slurry consisting of SSC–SDC with a weight ratio of 7:3 and a binder was screen-printed on the electrolyte surface and fired at 950 °C for 2 h to form single cells. The cathode fabricating process was kept as consistent as possible so that identical cathodic polarization resistance can be achieved [7,24]. The cell was sealed onto an alumina tube with silver paste (DAD-87, Shanghai Research Institute of Synthetic Resins). Humidified (3% H_2O) hydrogen was used as the fuel with a flow rate of 50 mL min^{-1} and ambient air as the oxidant. Electrochemical characterizations were performed at 600 °C under ambient pressure. An Electrochemical Workstation (IM6e, Zahner) was used to characterize single cells. The current–voltage curve was obtained by using a galvanostat mode and the electrochemical impedance spectra were measured at open circuit conditions in the frequency range from 0.1 Hz to 1 MHz with 5 mV as AC amplitude. The micro-structure was observed via a scanning electron microscope (SEM, JSM-6700F, JEOL).

4. Results and discussions

4.1. Model results and analysis

To conduct the model calculation, the radius of the e-particle (Ni) and i-particle (SDC) is assumed to be 0.5 and 0.05 μm, respectively. This assumption was made based on the microstructure observation of the coated-anode, which is discussed in the following section. In the previous reports on micro-models of SOFC electrodes, a relative low contact angle, $2\theta = 30°$, is generally assumed [25–27] since it is described as the contact angle between two particles of heterogeneous phases. The low angle assumption is possibly due to the fact that both Ni and NiO are not soluble in YSZ solid solutions. However, in the case of the model for an electrolyte-coated anode, $2\theta_1$ is the contact angle between two particles of homogonous phase. The angle is formed with high-temperature firing of two neighboring NiO particles. Therefore, a much higher contact angle will be expected. It is difficult to acquire accurate value of contact angles $2\theta_1$ but here we give different angles with 60°, 70° and 80°. For unified calculation hereafter, the contact angle of 60° is used. The contract angle between an i-particle and an e-particle is assumed to be $2\theta_2 = 30°$, which is the same as those reported. The density of i-particle, SDC, is 7.147 g cm^{-3} as determined with the lattice parameter calculated from X-ray diffraction pattern. The dependence of the exposed surface area of e-particles per unit volume, A_E, on porosity at different contact angles between e-particles is shown in Fig. 2. A_E is found to increase with the porosity at the range of 0.30–0.53, which is an usual porosity

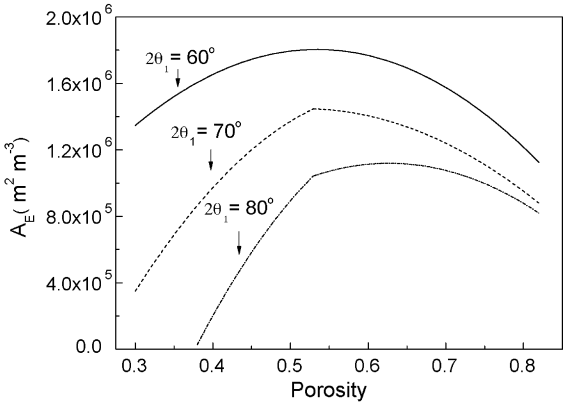

Fig. 2. The dependence of the exposed surface area of the e-particles per unit volume on porosity at different contact angles.

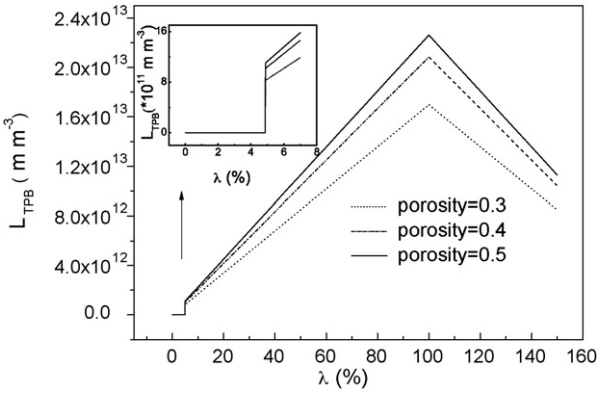

Fig. 3. The correlations between the length of three-phase-boundary per unit volume and the coverage at different porosities.

range for the anodes. The increasing A_E implies an increase in the maximum loading, i.e. more i-particles can be deposited on the surface of e-particles.

The correlations between the length of triple-phase-boundary per unit volume, L_{TPB}, and the coverage, λ, at different porosity are shown in Fig. 3. It is noted that when λ is relative small, i-particles do not belong to a percolated cluster and thus L_{TPB} is zero, meaning that the electrolyte coating does not contribute to the active reaction sites. On the other hand, $\lambda = 100\%$ means that the exposed surface is fully covered by i-particles with a monolayer. The full coverage corresponds to a maximum L_{TPB}. With the monolayer assumption, the maximum loading is calculated to be 599, 733 and 780 mg cm^{-3} for the substrates with porosity = 31, 42, and 54%, respectively. When $\lambda > 100\%$ or the loading exceeds these values, the e-particles are covered with multilayer i-particles. It should be noted that the multilayer coverage will not increase L_{TPB} value. On the contrary, it will decrease L_{TPB} by blocking gas diffusion. The curve shown in Fig. 3 when $\lambda > 100\%$ is plotted on the assumption that the overloaded i-particles are deposited onto the monolayer and gas transportation to/off the preformed boundary between the electron and ion conducting phases is blocked, and thus L_{TPB} is diminished with increased two-layer coverage. Based on Fig. 3 and Eq. (16), it can be concluded that:

(1) The length of the triple-phase-boundary is proportional to the coverage, and also to the loading when the e-particles are covered with monolayer i-particles and the i-particles are percolated at $\lambda > \lambda_{cr}$;
(2) At the same coverage, higher substrate porosity is related to longer length of the triple-phase-boundary;
(3) When the loading is smaller than the maximum value corresponding to full monolayer coverage, the length of the triple-phase-boundary is independent of the porosity, i.e. L_{TPB} is only determined by the loading.

Therefore, it is theoretically feasible that a larger TPB length can be obtained by improving the substrate porosity and the loading of i-particle.

4.2. Experimental results and analysis

4.2.1. Anode micro-structure

The substrate porosity increased with the amount of the pore former. The porosity before reduction was 31, 42 and 54% for FC10, FC20 and FC30, respectively. As shown in Table 1, increase in open porosity makes it easier to load SDC. The loading obtained with each cycle was about 71 mg cm^{-3} for FC10 [7]. The average values for FC20 and FC30 were approximately 94 and 130 mg cm^{-3}, respectively. As a result, it appears that for a given loading FC30 requires the least impregnating–heating cycles, which implies a simplified fabrication process [3].

SEM picture of the cross-section view for FC30 anode is shown in Fig. 4. The average size of NiO particles is close to 1 μm. After 648 mg cm^{-3} of SDC was impregnated, very fine and well dispersed SDC particles with an average diameter of ~100 nm were observed to be coated on the large particles. The distribution of SDC particles appears to be not only uniform but also continuous, which is important for ionic conducting within the electrode.

4.2.2. Fuel cell performance

The open circuit voltages (Vocs) at 600 °C were between 0.82 and 0.87 V, which were typical for SOFCs with thin film ceria as the electrolytes. The relative low Vocs are believed to be due to an internal short-circuit for the reduction of ceria and the effect of interfacial polarization resistance on a mixed-conducting film electrolyte [28].

The dependence of the cell voltage and power density on current densities at 600 °C with humidified (3% H_2O) hydrogen as the fuel is shown in Fig. 5. The data shown in Fig. 5a and b were measured with cells that were prepared with 20 and 30 wt.% pore former, respectively. The performance of the cell with 10 wt.% pore former has been reported previously [7]. The cell performance changes with the amount of coated SDC. Increasing the SDC loading can enhance the performance. A peak power density was observed for all the cells. As shown in Fig. 5b, when 30 wt.% pore former was applied and 648 mg cm^{-3} SDC was impregnated, the single cell (FC30-5) demonstrated the highest performance with 723 mW cm^{-2} of the peak power density. Similarly, 631 and 571 mW cm^{-2} of the peak power density were obtained with cells that were prepared with 20 and 10 wt.% starch, respectively.

The trend of change in cell performance is shown in Fig. 6 by presenting relationship between the peak power density and the SDC loading. In the case of FC30, the peak power density was 385 mW cm^{-2} when no SDC was impregnated. It increased to 498 mW cm^{-2} when 389 mg cm^{-3} of SDC was impregnated. The peak power density increases to the maximum value, 723 mW cm^{-2}, when 648 mg cm^{-3} of SDC was deposited. The same tendency was also observed on the cells whose anodes were prepared with 10 and 20 wt.% pore former. These indicate that the improvement in the cell performance originates from the prolonged length of TPB by increasing the SDC loading, which is in good agreement with the result from our model as discussed previously. However, further increase in the loading lowered the cell performance. As demonstrated

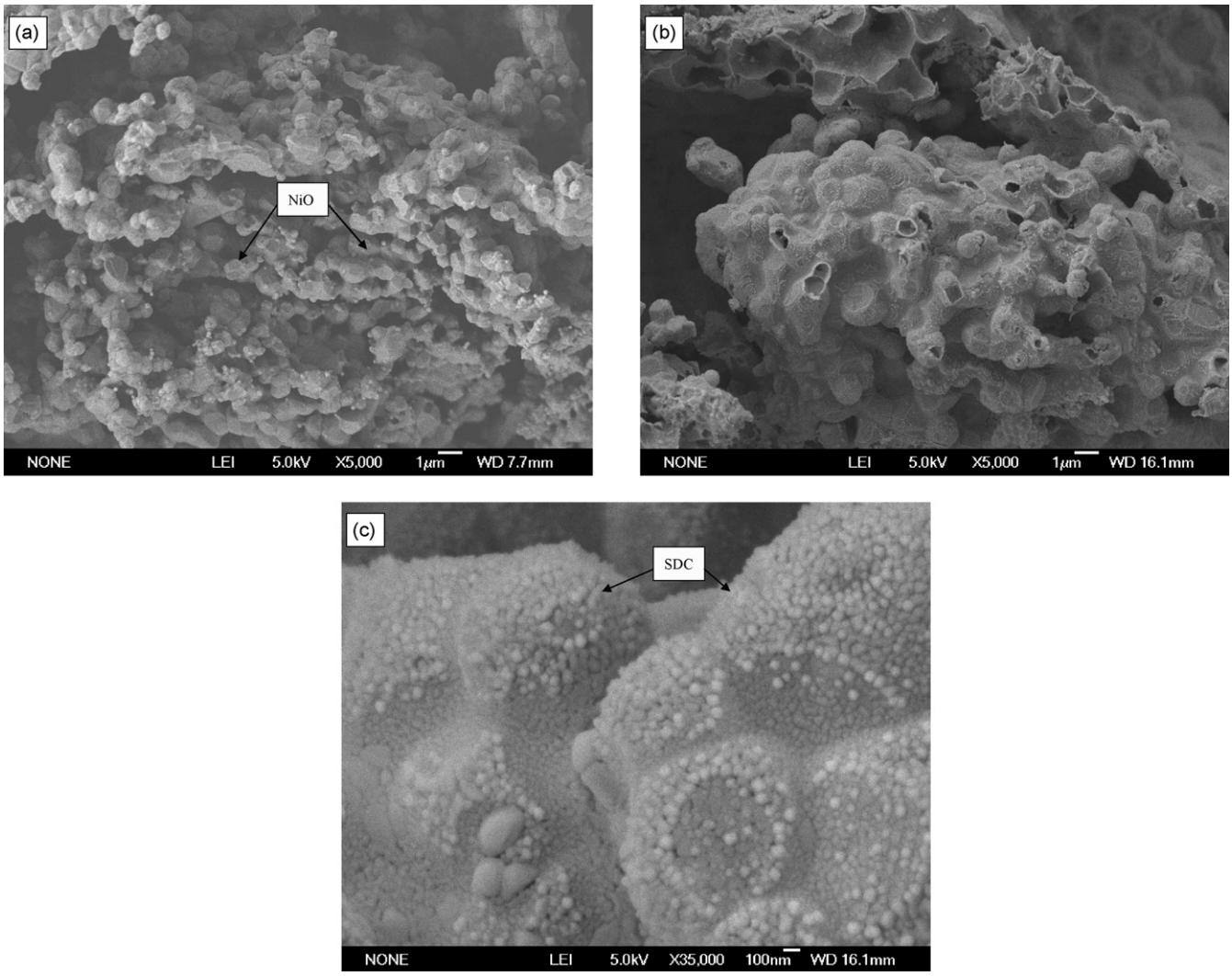

Fig. 4. SEM micrographs for FC30: (a) substrate, (b) loaded with 648 mg cm^{-3} of SDC and (c) high magnification for (b).

in Fig. 3, the presence of the multilayer deposition results in a decrease in L_{TPB}. Therefore, the decrease in peak power density is associated with L_{TPB} reduction as a result of insufficient gas supply.

The model demonstrates previously that increased porosity enables more SDC particles to be deposited so that L_{TPB} per unit volume can be prolonged. For example, when the porosity increases from 0.3 to 0.5, L_{TPB} increases with the loading till $\lambda = 100\%$. Consequently, an increase in the highest peak power density with porosity is expected. This can be clearly seen in Fig. 6. The ratio of the highest peak power density of FC10, FC20, and FC30 is 1:1.09:1.27 while the ratio of L_{TPB} for the anode in FC10, FC20 and FC30 is 1:1.22:1.29, calculated based on Eq. (16) when $\lambda = 100\%$. Considering the fact that the highest peak power density might be achieved at SDC loading slightly different with that as shown in Fig. 6, it seems to have some quantitative relationship between the highest peak powder density and L_{TPB} per unit volume. It should be noted that too high porosity will result in with very poor mechanical strength. Note also that the loadings related to the highest peak power density are smaller than that derived from the calculation at $\lambda = 100\%$ with an assumption that $2\theta_1 = 60^\circ$. This is possibly due to the choice of the angle contact. For example, when the contact angle of 70° is adopted, the calculated maximum loading is 182, 463 and 624 mg cm^{-3}, respectively, which are smaller than the experimental values.

Before the highest peak power density is achieved, it can be found that the peak power density is nearly equal although the porosity is different, especially in the case of FC10 and FC20. It is consistent with the conclusion that the same loading results in the same L_{TPB} when $\lambda = 100\%$. The fitted curves shown in Fig. 6 indicate that almost no improvement in cell performance would be expected when the loading is low, for example, 10 mg cm^{-3}. This situation agrees well with the model simulation when Figs. 6 and 3 are compared. The predicted SDC loading for the percolation threshold is 29, 36 and 38 mg cm^{-3} for FC10, FC20 and FC30, respectively.

4.2.3. Resistance of the anode/electrolyte interfaces

Typical impedance spectra for the FC20 and FC30 measured under open circuit conditions at 600 °C using a two-electrode configuration are shown in Fig. 7a and b. Since the electronic

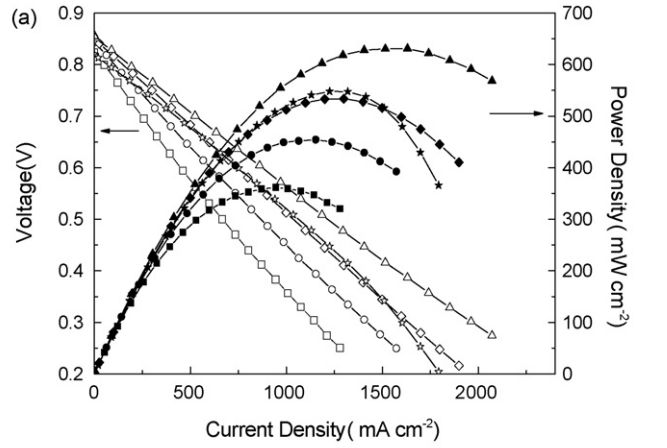

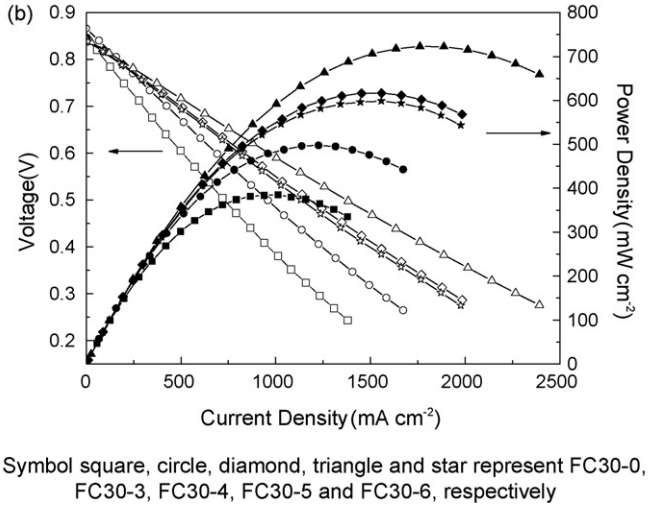

Fig. 5. Dependence of the cell voltage and power density on current density at 600 °C for (a) FC20 and (b) FC30 with humidified (3% H_2O) hydrogen as the fuel.

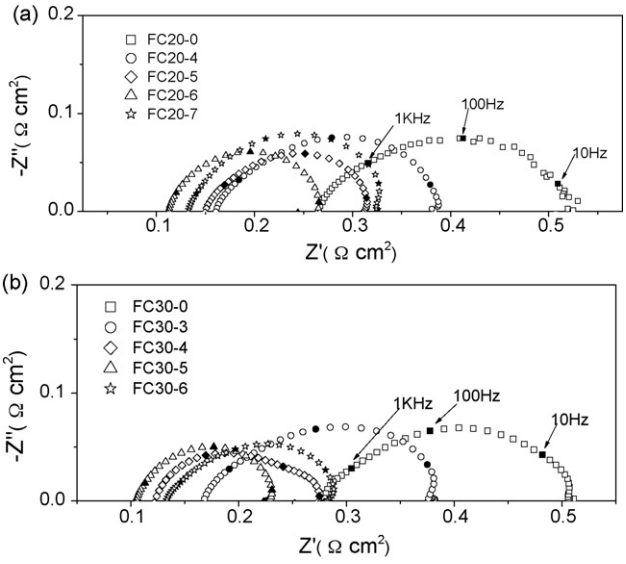

Fig. 7. Impedance spectra measured at an open circuit condition for (a) FC20 and (b) FC30.

conduction in SDC electrolyte is not negligible under the fuel cell condition, the interfacial polarization resistance (R_p) must be adjusted according to the following equation [28,29]:

$$R_p = \frac{R_t - R_o}{(V_{oc}/E_N)[1 - (R_o/R_t)(1 - (V_{oc}/E_N))]} \quad (17)$$

where V_{oc} is the open circuit voltage, E_N the Nernst potential across the cell. The ohmic resistance, R_o, measured from the high frequency intercept with the real axis, is primarily contributions from the electrolyte. R_t is the intercept of the impedance with the real axis at low frequency. It is difficult to separate the anodic polarization resistance, R_a, from the cathodic one because of the complexity of the impedance spectra obtained with an anode-supported cell [30]. The variation of R_p, however, can be considered to be only derived from that of R_a since the cathode fabricating process was kept as consistent as possible so that the cathodic polarization resistance can be identically achieved. Fig. 8 shows the variation of R_p with SDC loading for FC20 and FC30. For FC20, R_p decreased from 0.330 Ω cm^2 when no

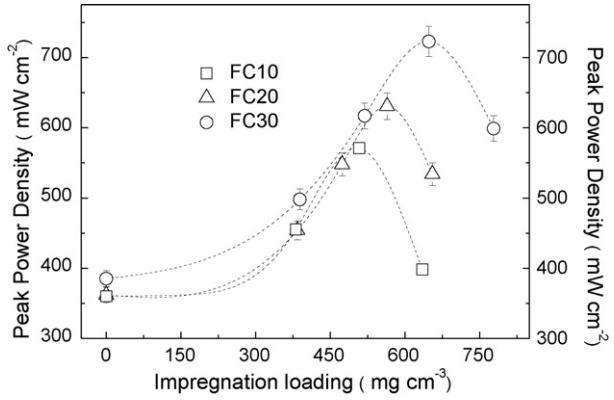

Fig. 6. Dependence of the peak power density on SDC loading for cell prepared with different amount of pore former (The data of FC10 are derived from Ref. [7].).

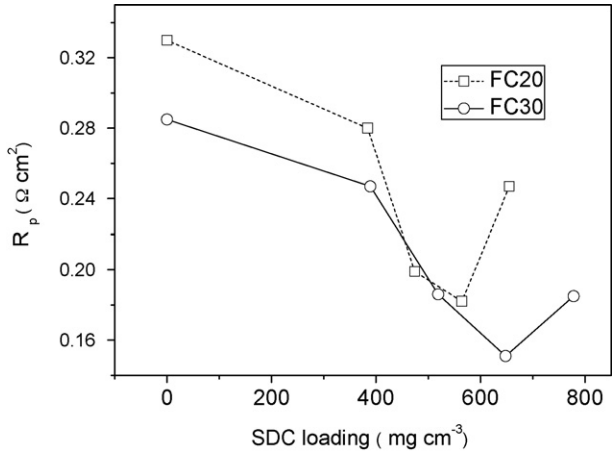

Fig. 8. The variation of R_p with SDC loading.

SDC was coated to 0.182 Ω cm^2 when 564 mg cm^{-3} of SDC was deposited. In the case of FC30, R_p was 0.285 Ω cm^2 for the cell without any coated SDC. With 648 mg cm^{-3} of deposited SDC, R_p was reduced to 0.151 Ω cm^2. The decrease in R_p is 0.148 and 0.134 Ω cm^2, respectively, and is 45 and 47% of R_p for the corresponding cells without impregnation. The change of interfacial polarization resistance versus SDC loading agrees well with the variation of peak power density versus the loading. It is clear that the improvement of cell performance is primarily due to the decrease of R_a as an effect of pronounced triple-phase boundary caused by impregnating–heating treatment.

It can be observed that the ohmic resistance, R_o, was also significantly reduced after impregnating–heating treatment. Take FC30 as an example, R_o decreased from 0.278 Ω cm^2 for FC30-0 to 0.105 Ω cm^2 for FC30-4. It is possibly accounted for the enlargement of contact area at the anode/electrolyte interface by means of the impregnation process. Wanzenberg et al. [31] found that the measured conductivity of YSZ film electrolyte was low compared to that of the YSZ bulk material previous reported. They attributed this to the relative small contact area between the porous electrode and electrolyte derived from the electrode pore and the roughness of the electrolyte surface. In our work, when no SDC was deposited, open pores with high pore volume derived from pore former make this contact area not continuous but consist of discrete point contacts. After impregnating–heating treatment, nano-sized SDC particles enlarge significantly the contact area between the ionic phase and electronic phase. Consequently, R_o is substantially reduced. Vanberkel et al. [32] also pointed out that smaller particles at the electrode/electrolyte interface could make for larger area that was involved in faster reaction kinetics and higher currents that could be drawn through the electrode. It is noted that too much impregnated-SDC, such as FC30-5 with 778 mg cm^{-3} of the loading, caused an increase in R_o and R_p which resulted in a decrease of the cell performance. This suggested that excessive SDC loading may increase ionic resistance and decrease L_{TPB}, therefore reduce the cell performance.

5. Conclusions

We demonstrate a strategy to achieve the anode with high performance via not only a micro-model but also experiments. A geometric micro-model for the electrolyte-coated anode is developed according to a random packing system and an assumption of monolayer coverage. The model shows that the length of triple-phase-boundary depends on the porosity and the impregnation loading when an ion impregnation method is used to fabricate the anode. In the porosity range of 0.3–0.5, the maximum loading increases with porosity. Hence, the prolonged TPB length per unit volume can be achieved by improving the porosity and the loading. In experiments, Ni was used as electron conducting matrix and SDC as ion conducting impregnation. The highest peak power density of the cells whose anode prepared with 10, 20 and 30 wt.% pore former was 571, 631 and 723 mW cm^{-3}, respectively at 600 °C when hydrogen was used as the fuel. The experiment showed good agreement with the model, providing some insight into the optimization of the electrode.

Acknowledgement

This work was supported by the Natural Science Foundation of China (50672096 and 50730002).

References

[1] A. Atkinson, S. Barnett, R.J. Gorte, J.T.S. Irvine, A.J. Mcevoy, M. Mogensen, S.C. Singhal, J. Vohs, Nat. Mater. 3 (2004) 17.
[2] R.J. Gorte, S. Park, J.M. Vohs, C.H. Wang, Adv. Mater. 12 (2000) 1465.
[3] S.P. Jiang, Mater. Sci. Eng. A-Struct. Mater. Prop. Microstruct. Process. 418 (2006) 199.
[4] S.P. Yoon, J. Han, S.W. Nam, T.H. Lim, S.A. Hong, J. Power Sources 136 (2004) 30.
[5] B. Huang, X.F. Ye, S.R. Wang, H.W. Nie, R.Z. Liu, T.L. Wen, Mater. Res. Bull. 42 (2007) 1705.
[6] S. Zhao, R.J. Gorte, Appl. Catal. A-Gen. 277 (2004) 129.
[7] W. Zhu, C.R. Xia, J. Fan, R.R. Peng, G.Y. Meng, J. Power Sources 160 (2006) 897.
[8] B. Huang, X.F. Ye, S.R. Wang, H.W. Nie, J. Shi, Q. Hu, J.Q. Qian, X.F. Sun, T.L. Wen, J. Power Sources 162 (2006) 1172.
[9] S.P. Jiang, S. Zhang, Y. Da Zhen, W. Wang, J. Am. Ceram. Soc. 88 (2005) 1779.
[10] S.P. Jiang, S. Zhang, Y.D. Zhen, A.P. Koh, Electrochem. Solid-State Lett. 7 (2004) A282.
[11] J. Mizusaki, H. Tagawa, T. Saito, T. Yamamura, K. Kamitani, K. Hirano, S. Ehara, T. Takagi, T. Hikita, M. Ippommatsu, S. Nakagawa, K. Hashimoto, Solid State Ionics 70 (1994) 52.
[12] A. Bieberle, L.J. Gauckler, Solid State Ionics 135 (2000) 337.
[13] X.H. Deng, A. Petric, J. Power Sources 140 (2005) 297.
[14] P. Costamagna, P. Costa, V. Antonucci, Electrochim. Acta 43 (1998) 375.
[15] J. Abel, A.A. Kornyshev, W. Lehnert, J. Electrochem. Soc. 144 (1997) 4253.
[16] C.W. Tanner, K.Z. Fung, A.V. Virkar, J. Electrochem. Soc. 144 (1997) 21.
[17] S. Sunde, J. Electroceram. 5 (2000) 153.
[18] S.H. Chan, Z.T. Xia, J. Electrochem. Soc. 148 (2001) A388.
[19] J.H. Nam, D.H. Jeon, Electrochim. Acta 51 (2006) 3446.
[20] M. Suzuki, K. Makino, M. Yamada, K. Linoya, Int. Chem. Eng. 21 (1981) 482.
[21] M. Suzuki, T. Oshima, Powder Technol. 35 (1983) 159.
[22] A. Malliaris, D.T. Turner, J. Appl. Phys. 42 (1971) 614.
[23] C.R. Xia, M.L. Liu, Solid State Ionics 144 (2001) 249.
[24] Z. Xie, C. Xia, M. Zhang, W. Zhu, H. Wang, J. Power Sources 161 (2006) 1056.
[25] P. Costamagna, P. Costa, E. Arato, Electrochim. Acta 43 (1998) 967.
[26] X.J. Chen, S.H. Chan, K.A. Khor, Electrochim. Acta 49 (2004) 1851.
[27] S.H. Chan, X.J. Chen, K.A. Khor, J. Electrochem. Soc. 151 (2004) A164.
[28] M.L. Liu, H.X. Hu, J. Electrochem. Soc. 143 (1996) L109.
[29] S. Zha, W. Rauch, M. Liu, Solid State Ionics 166 (2004) 241.
[30] S. McIntosh, J.M. Vohs, R.J. Gorte, J. Electrochem. Soc. 150 (2003) A1305.
[31] E. Wanzenberg, F. Tietz, D. Kek, P. Panjan, D. Stover, Solid State Ionics 164 (2003) 121.
[32] F.P.F. Vanberkel, F.H. Vanheuveln, J.P.P. Huijsmans, Solid State Ionics 72 (1994) 240.